JCI The Journal of Clinical Investigation

Auxiliary trafficking subunit GJA1-20k protects Connexin43 from degradation and limits ventricular arrhythmias

Shaohua Xiao, … , TingTing Hong, Robin M. Shaw

J Clin Invest. 2020. https://doi.org/10.1172/JCI134682.

Research In-Press Preview Cardiology Cell biology

Graphical abstract

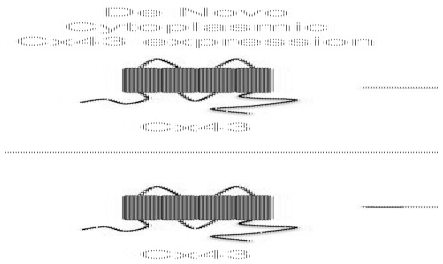

Auxiliary Trafficking Subunit GJA1-20k Protects Connexin43 from Degradation and Limits Ventricular Arrhythmias

Shaohua Xiao,[1,2,*] Daisuke Shimura,[1,*] Rachel Baum,[1,3] Diana M Hernandez,[3] Sosse Agvanian,[3] Yoshiko Nagaoka,[3,4] Makoto Katsumata,[3] Paul D Lampe,[5] Andre G Kleber,[6] TingTing Hong,[1,3] Robin M Shaw[1]

[1]Nora Eccles Harrison Cardiovascular Research and Training Institute, University of Utah, Salt Lake City, UT, USA

[2]Department of Neurology, University of California at Los Angeles, Los Angeles, CA, USA

[3]Department of Biomedical Sciences, Cedars-Sinai Medical Center, Los Angeles, CA, USA

[4]Department of Pathology, University of Alabama at Birmingham, Birmingham, AL, USA

[5]Translational Research Program, Public Health Sciences and Human Biology Divisions, Fred Hutchinson Cancer Research Center, Seattle, WA, USA

[6]Department of Pathology, Beth Israel Deaconess Medical Center, Harvard Medical School, Boston, MA, USA

*These authors contributed equally to this work: SX, DS

Address correspondence to:

Robin M Shaw

Nora Eccles Harrison Cardiovascular Research and Training Institute

University of Utah

95 South 2000 East, Suite 143

Salt Lake City, UT 84112

USA

Phone: 801-581-8183

Email: Robin.Shaw@hsc.utah.edu

Conflict of Interest

The authors have declared that no conflict of interest exists.

Abstract

Connexin 43 (Cx43) gap junctions provide intercellular coupling which ensures rapid action potential propagation and synchronized heart contraction. Alterations in Cx43 localization and reductions in gap junction coupling occur in failing hearts, contributing to ventricular arrhythmias and sudden cardiac death. Recent reports have found that an internally translated Cx43 isoform, GJA1-20k, is an auxiliary subunit for the trafficking of Cx43 in heterologous expression systems. Here, we have created a mouse model by using CRISPR technology to mutate a single internal translation initiation site in Cx43 (M213L mutation), which generates full length Cx43 but not GJA1-20k. We found that *GJA1*$^{M213L/M213L}$ mice had severely abnormal electrocardiograms despite preserved contractile function, reduced total Cx43, reduced gap junctions, and died suddenly at two to four weeks of age. Heterozygous *GJA1*$^{M213L/WT}$ mice survived to adulthood with increased ventricular ectopy. Biochemical experiments indicated that cytoplasmic Cx43 had a half life that was 50% shorter than membrane associated Cx43. Without GJA1-20k, poorly trafficked Cx43 was degraded. The data support that GJA1-20k, an endogenous entity translated independently of Cx43, is critical for Cx43 gap junction trafficking, maintenance of Cx43 protein, and normal electrical function of the mammalian heart.

Introduction

Intercellular communication between cardiomyocytes via connexin 43 (Cx43) gap junctions enables the rapid spread of electrical signals and synchronous ventricular contraction. Oligomerization of six Cx43 molecules gives rise to a connexon or hemichannel, which binds to a connexon from the adjacent cell to form a full gap junction channel. Cx43 gap junction channels are primarily localized to the intercalated discs (ICDs) at the longitudinal ends of cardiomyocytes (1). Loss of Cx43 gap junction coupling contributes to abnormal propagation of electrical impulse, arrhythmias, and sudden cardiac death (2, 3). Similar to other cardiac ion channels, Cx43 has a short half-life ranging from 1 to 3 hours (4, 5). Given the importance of properly localized Cx43 at gap junctions and its rapid turnover, forward trafficking and localization of Cx43 is under intricate regulation that is only beginning to be understood.

In heterologous expression systems, it has been identified that a short isoform of Cx43, GJA1-20k, serves as a chaperone for the assembly and trafficking of full length Cx43 gap junction channels (5-8). The GJA1-20k isoform is produced as a result of alternative translation of mRNA, by which AUG codons (typically coding for Methionine) within the coding region of the *GJA1* mRNA function as ribosomal start sites to initiate translation. Thus protein formation can be initiated downstream of the canonical translation start site, generating N-terminal truncated protein isoforms (6). GJA1-20k is the most abundant internally translated Cx43 isoform endogenously expressed in the heart (6). In isolated cells, full length Cx43 introduced heterologously by plasmids whose corresponding mRNA is unable to generate GJA1-20k, fail to be delivered to cell-cell junctions, while addition of exogenously expressed GJA1-20k rescues the trafficking defects of full length protein (6). The facilitation of GJA1-20k in forward

trafficking is related to its interaction with the cytoskeleton, which serves as the membrane protein delivery apparatus. GJA1-20k organizes the actin and microtubule cytoskeleton for targeted delivery of Cx43 hemichannels to cell-cell borders (7). Despite knowledge of GJA1-20k participation of Cx43 trafficking, the life cycle of Cx43 channels in adult heart cells remains poorly understood. It is not known if channels in the plasma membrane behave differently than those not yet delivered. If channels can not be trafficked, can they remain available in the cardiomyocyte or are they degraded?

The questions regarding Cx43 movement and life cycle have immediate relevance to cardiac health. If Cx43 channels are limited in their ability to traffic to the cardiac ICD, do they remain available for ultra-rapid delivery post a stimulus, or would new channels need to be generated prior to enhancement of gap junction coupling? How prepared are mammalian hearts for a sudden need for increased intercellular coupling? We have found that actin stabilization and pretreatment with GJA1-20k can preserve coupling in adult hearts subsequently subjected to ischemic stress (7, 9). Pretreatment with GJA1-20k is also cardioprotective (10). Understanding the role of GJA1-20k in regulating Cx43 will guide therapies for gap junction rescue, such as helping to determine whether therapeutic interventions could be immediately effective post the start of ischemia or require initiation of treatment prior to the onset of an ischemic period.

To explore the movement of Cx43 *in vivo* and in adult cardiomyocytes, we generated a mouse model deprived of GJA1-20k using the CRISPR homology directed repair (HDR) technology to mutate the single internal methionine initiation codon for GJA1-20k (GJA1-M213L mutation, corresponding to substitution of AUG by UUA in mRNA). This mutation is in a highly

conserved region of Cx43 DNA which does not affect production of full length Cx43, but removes endogenous generation of GJA1-20k. The results are that, without its smaller trafficking partner, full length Cx43 does not reach the ICD and mice without GJA1-20k formation die from apparent sudden cardiac death. Surprisingly, we find that poorly trafficked Cx43 is degraded rather than stored in cytoplasmic reserves. The stability of ICD associated Cx43 is much higher than that of cytoplasmic Cx43.

Results

$GJA1^{M213L/M213L}$ mice die suddenly.

To explore perturbation of Cx43 trafficking *in vivo*, we created a mouse model that reduced the ability of GJA1-20k to be formed by replacing the internal ribosomal translation start site, the AUG encoding amino acid 213 (Methionine213) of the mouse Cx43, to UUA (encoding Leucine, L). We used CRISPR-HDR technology to edit the genomic sequence at the target location (Figure 1A and Supplemental Figure 1). The sequence around the target site in the wild type (WT) allele is sensitive to NlaIII restriction digestion, whereas that in the M213L mutated allele is resistant. Therefore, PCR amplification and NlaIII digestion produced 2, 3, and 1 DNA fragments in the genotyping assay of WT, heterozygotes (HT), and homozygotes (HM), respectively (Figure 1B). The M213L mutation did not significantly change the expression level of the *GJA1* mRNA (Figure 1C). However, the expression of the GJA1-20k protein was almost completely removed in mice homozygous for the M213L mutation compared to the WT and HT littermates (Figure 1, D and E). These observations are consistent with previous studies in heterologous expression systems, demonstrating that the GJA1-20k protein is produced as a result of alternative translation initiation (6, 11, 12). Taken together, the level of endogenous GJA1-20k protein was effectively diminished in mice carrying M213L mutation. We thus refer this mouse model as a $GJA1^{M213L/M213L}$ for the homozygous mutant and $GJA1^{M213L/WT}$ for the heterozygous mutant.

It should be emphasized that while our use of the terms “homozygous”, “heterozygous”, and “mutation” is technically correct, these terms typically refer to mutations in genes that are associated with an absence or change in the corresponding full length protein. In the case of our

M213L mutation, we are changing an internal ribosomal start site. Even for the homozygous *GJA1*$^{M213L/M213L}$ mouse, full length Cx43 mRNA and protein are still generated yet there is decreased internal ribosomal translation and decreased production of the smaller GJA1-20k protein. As a result, any changes to Cx43 expression with an M213L mutation are therefore secondary to post-translational Cx43 movements and processing in the presence of unchanged primary synthesis yet reduced GJA1-20k.

The *GJA1*$^{M213L/M213L}$ mice grew similarly to the WT and heterozygous littermates for two weeks, without difference in gross physical appearance (Figure 2, A-C). However, they died suddenly around 2-4 weeks old, with the median life span of 18 days (Figure 1F). In addition, young *GJA1*$^{M213L/M213L}$ mice did not show abnormalities in the right ventricular outflow tract (RVOT) or in other cardiac regions, although it was previously reported that a mouse lacking full-length Cx43 develops RVOT outflow tract obstruction and death at birth (13). The survival to 2-4 weeks (Figure 1F) and normal physical development (Figure 2, A-C) argues against RVOT outflow tract obstruction. We also performed echocardiography on these mice at two to three weeks of age (Figure 2D) and found normal left ventricular (LV) and right ventricular (RV) size and function, indicating preserved hemodynamics despite a loss of GJA1-20k. Full echocardiographic parameters of the young mice are presented in Table 1, which indicates that heart rate, as well as all 13 other structural and functional parameters of the heart are not changed among WT, *GJA1*$^{M213L/WT}$, and *GJA1*$^{M213L/M213L}$ mice. The only significant difference is the long axis fractional shortening which is mildly reduced in *GJA1*$^{M213L/M213L}$ mice (12.96 ± 1.17%) compared to WT (19.11 ± 1.07%) and *GJA1*$^{M213L/WT}$ (18.78 ± 1.07) littermates (Table 1). Overall ejection fraction as well as LV systolic and diastolic volumes are unchanged (Table 1).

Although *GJA1*$^{M213L/M213L}$ mice die young, we were able to measure echocardiographic parameters to assess the structure and hemodynamics of the *GJA1*$^{M213L/WT}$ and WT adult mouse hearts. In mice 9-10 weeks old, only LV end diastolic volume is significantly yet mildly reduced in *GJA1*$^{M213L/WT}$ (43.61 ± 2.26 μL) compared to WT littermates (55.52 ± 3.65 μL). All 13 other structural and functional parameters are unchanged (supplemental Table 1). The echocardiographic data are reassuring that structural and mechanical parameters are not significantly affected by the M213L mutation, further indicating that impaired mechanical cardiac function cannot explain the early sudden death phenotype of *GJA1*$^{M213L/M213L}$ mice.

GJA1$^{M213L/M213L}$ *and GJA1*$^{M213L/WT}$ *mice have abnormal cardiac electrical excitation.*

We explored differences in electrical function as a potential mechanism of the sudden death of *GJA1*$^{M213L/M213L}$ mice, as illustrated in Figure 3. Electrocardiograms (ECGs) were recorded to examine cardiac whole heart excitation in anesthetized *GJA1*$^{M213L/M213L}$ and *GJA1*$^{M213L/WT}$ mice. In young mice (2-3 weeks of age), a paucity of GJA1-20k results in a greatly reduced R wave amplitude. WT (0.8740 ± 0.05465 mV, mean ± SEM) R wave amplitude is reduced by 16% in *GJA1*$^{M213L/WT}$ mice (0.7360 ± 0.03750 mV), and by a remarkable 92% in *GJA1*$^{M213L/M213L}$ mice (0.06773 ± 0.01391 mV) (Figure 3, A-C). Duration of the QRS complexes is tripled in the *GJA1*$^{M213L/M213L}$ mice (38.57 ± 5.98 ms) compared to WT mice (12.97 ± 0.57 ms) (Figure 3, A-C), indicating impaired ventricular excitation, probably as a result of global propagation slowing (14). Next, we used implanted telemetry to monitor ECGs of conscious and active adults (6-7 months old) WT and *GJA1*$^{M213L/WT}$ mice. The heterozygotes developed significantly more premature ventricular contractions (PVCs) than WT mice (Figure 3D). The average number of

ectopic incidents per hour (including single PVCs and 2-4 consecutive PVCs) was 141.7 ± 23.16 (mean ± SEM) in *GJA1*$^{M213L/WT}$ mice vs. 23.40 ± 8.45 in WT (Figure 3E). The decrease in R wave amplitude, lengthening of QRS complex duration, and increase in frequency of PVCs indicate that, even in *GJA1*$^{M213L/WT}$ animals, cardiac electric excitation is impaired when GJA1-20k expression is reduced.

Expression of full-length Cx43 at the intercalated discs (ICDs) is reduced in GJA1$^{M213L/M213L}$ *mutant mouse hearts with GJA1-20k depletion.*

Since GJA1-20k has been shown to facilitate delivery of full-length Cx43 to cell-cell junctions in cultured cell lines and primary cardiomyocytes (6, 7) and reduced expression of Cx43 is associated with decreased voltage in QRS complexes (15-17), we examined the expression of Cx43 at the ICDs in *GJA1*^{M213L} mutant mouse hearts, as depicted in Figure 4. Indeed, full-length Cx43 has minimum expression at the ICDs, in contrast to the expected localization at ICDs in WT hearts (Figure 4A). Quantification of the Cx43 signal at the ICDs, which were delineated by N-cadherin staining, revealed a 53.9% reduction in *GJA1*$^{M213L/M213L}$ (462.7 ± 20.71 units) vs. WT (1004 ± 65.02 units) (Figure 4B). In heterozygous *GJA1*$^{M213L/WT}$ cardiomyocytes, Cx43 was similar to WT hearts (Figure 4, A and B). As expected (18, 19) there was no difference in N-cadherin expression among WT, HT, and HM hearts (Supplemental Figure 2), which suggests that the impairment of Cx43 localization to ICDs may result from impaired forward trafficking of hemichannels to the otherwise intact disc (20). Total Cx43 protein in the ventricles was also explored by Western blot (Figure 4C) and quantified (Figure 4D). The reduction of Cx43 in adult myocardium of *GJA1*$^{M213L/M213L}$ mice is surprisingly severe (Figure 4D), despite unaltered levels of Cx43 mRNA (Figure 1C), attributing this Cx43 reduction to a post-transcriptional

event. This is in line with an earlier finding of rescue of full length Cx43 localization at the ICD by GJA1-20k alone even when Cx43 had a M213L mutation (6). Therefore, the loss of Cx43 in the *GJA1*$^{M213L/M213L}$ mice is a post-translational effect on Cx43, reflecting increased protein degradation.

Cx43 gap junctions are responsible for the cell-to-cell spatial spread of electrotonic current in ventricular muscle. Severely reduced Cx43 gap junction localization to intercalated discs would cause delayed excitation, explaining the reduced QRS amplitudes with QRS notching and widening seen in Figure 3. Once membrane electrotonic downstream current has reached the threshold for sodium channels (Nav1.5) activation, the sodium current, as the main charge carrier, will produce the action potential upstroke and further downstream flow of electrotonic currents (21). This crucial complimentary role of Cx43 and Nav1.5 prompted us to explore, whether loss of GJA1-20k affects sodium channel localization at the ICD as well. In the *GJA1*$^{M213L/M213L}$ mice and *GJA1*$^{M213L/WT}$ mice, sodium channel localization does not appear to be affected (Figure 4, E and F). There is also no change in overall sodium channel protein (Figure 4, G and H). These results indicate that the GJA1-20k effect is not necessary for sodium channel trafficking.

M213L mutation affects full-length Cx43 forward delivery to cell-cell junctions.

As described in Figure 4, the levels of full-length Cx43 protein are markedly reduced in the hearts of *GJA1*$^{M213L/M213L}$ mice compared to WT hearts, whereas the Cx43 expression level in *GJA1*$^{M213L/WT}$ mice is intermediate (Figure 4D). We explored whether the decrease of cellular Cx43 protein occurred in the cytoplasmic compartment of 2-3 weeks old mice ventricular

cardiomyocytes or by loss of Cx43 at the ICD. Triton fractionation was performed to separate and quantify the soluble (cytoplasmic) fraction of Cx43 from the insoluble (intercalated disc) fraction (18) (Figure 5). The results indicate that while the reduction of Cx43 at the intercalated disc is striking in *GJA1*$^{M213L/M213L}$ mice (Figure 5C), the amount of poorly trafficked Cx43 in the cytoplasm is slightly increased but still surprisingly close to that of WT mice. In Figure 5D we compare, for the WT (left column) and *GJA1*$^{M213L/M213L}$ (right column) mice, the relative contribution of ICD disc Cx43 (dark regions) and cytoplasmic Cx43 (light regions) to total Cx43 protein. In WT mice, there are roughly similar amounts of Cx43 at the ICD and in the cytoplasm. In *GJA1*$^{M213L/M213L}$ mice the reduction in Cx43 protein is due to reduction in ICD Cx43, without a compensatory increase in cytoplasmic Cx43, implying that the Cx43 that is not trafficked to the ICD is degraded.

The results of Figure 5 are supportive of a model that loss of GJA1-20k impairs forward trafficking of full-length Cx43 to the ICDs, which has already been established in cell lines and neonatal cardiomyocytes (6). However we now find that failure of Cx43 forward trafficking leads to faster Cx43 protein degradation, suggesting that the pool of cytoplasmic Cx43 is degraded faster than the pool of Cx43 successfully trafficked to the ICD. It is theoretically possible that the M213L mutation itself compromises cytoplasmic protein stability. To explore whether the different degradation rates for cytoplasmic Cx43 versus ICD Cx43 could be due to instability induced by the M213L mutation, we used pulse-chase experiments to assess protein stability of full-length mouse Cx43 with and without the M213L mutation (Figure 6). In HEK293 cells, we exogenously expressed either WT *GJA1* or GJA1-M213L plasmids, both tagged with human influenza hemagglutinin (HA). As expected, presence of the M213L

mutation results in reduced translation of GJA1-20k, as indicated by the reduced levels of GJA1-20k protein (Supplemental Figure 3). Furthermore, the stability of full-length WT Cx43 and mutated Cx43-M213L are similar (Figure 6, A-C). In the Triton-soluble (cytoplasmic) fraction, the time constant, tau (τ), of WT Cx43 and Cx43-M213L were similar, at 3.39 and 3.53 hours, respectively (Figure 6C). In fact the M213L mutation results in a slightly longer time constant. In the Triton-insoluble fraction, the τ of WT Cx43 and Cx43-M213L are also similar, at 4.95 and 5.34 hours, respectively (Figure 6C). Even in the membrane fraction, τ of Cx43-M213L is slightly longer than that of WT Cx43.

The data of Figure 6 indicate that the M213L mutation does not decrease Cx43 protein stability. However, when comparing τ between cytoplasmic and membrane fractions, it is striking that for both WT and mutated Cx43, Cx43 protein is 46% and 51% more stable in the Triton-insoluble fraction than in the Triton-soluble fraction (Figure 6 C). These results provide reassurance that the M213L mutation does not decrease protein stability. Instead, there is more rapid degradation of poorly trafficked, cytoplasmic Cx43. Given similar mRNA and protein production rates (Figure 1C and first column of Figure 6A), the shortened half life of cytoplasmic Cx43 results in less overall protein when Cx43 is not trafficked to the ICD (Figure 5D). These observations are consistent with a model where the pool of cytoplasmic Cx43 in the adult heart is degraded faster than the pool of ICD Cx43. When delivery of full-length Cx43 to the membrane is compromised due to the decrease in GJA1-20k mediated trafficking, there is faster degradation of Cx43. In the simplest sense, Cx43 not trafficked to the ICD is degraded, resulting in decreased ICD protein and similarly decreased total Cx43 protein.

M213L mutation affects non-cardiac Cx43.

Cx43 is the most common of 21 human connexin proteins, with roles in physiological processes that range from reproduction and development to coordination of central nervous system activity. In our mouse models, the M213L mutation is located at the endogenous *GJA1* gene. Thus, the mutated *GJA1* mRNA is expressed in tissues where the *GJA1* promoter is active. We quantified birth rate when breeding heterozygous animals and identified a non-Mendelian proportion of neonates with less *GJA1*$^{M213L/WT}$, and *GJA1*$^{M213L/M213L}$ pups relative to the number of *GJA1*$^{WT/WT}$ littermates (Figure 7A). We also explored Cx43 levels in mouse brain. We found, consistent with our findings in mouse hearts, that there is a similar amount of *GJA1* mRNA in the brains of *GJA1*$^{M213L/M213L}$ animals (Figure 7B) yet with a reduction of Cx43 protein (Figure 7, C and D) compared to WT littermates.

Discussion

To explore the role of the short Cx43 isoform GJA1-20k in Cx43 trafficking, we generated a mouse model deprived of GJA1-20k using the CRISPR homology directed repair (HDR) technology to mutate the single internal methionine initiation codon for GJA1-20k (GJA1-M213L mutation). At the level of the whole animal, GJA1-20k depletion revealed highly abnormal electrocardiographic parameters, a high incidence of sudden death, and increased incidence of premature ventricular contractions. At the cellular level, localization of Cx43 to ICDs is greatly reduced in the absence of GJA1-20k. We attributed the marked increase in total ventricular activation time and the decrease in QRS amplitude to a decrease in Cx43 (as the main ventricular connexin) because the level of Nav1.5 at the ICD, the other important determinant of the changes in the QRS complex, remained unchanged.

To our knowledge, the *GJA1*$^{M213L/M213L}$ mouse model we generated is the first in vivo model lacking an important Cx43 trafficking subunit (GJA1-20k) while retaining full length Cx43 protein. Yet there is a complementary precedent of our work. Published results involving truncated portions of the Cx43 C-terminus suggested that the C-terminus is needed to promote forward trafficking to the ICD. Cell line evidence of an independent truncated 20 kDa C-terminus band from Cx43 was first reported by the Delmar lab (8) showing that there is a significant reduction in Cx43 and a 20kDa band in cells and mice lacking *GJA1*. Additionally, using a mouse containing a truncation at amino acid 258 (Cx43KO258Stop) (22), and crossing Cx43258Stop with a Cx43 knockout mouse resulted in Cx43258Stop/KO animals surviving after birth. These Cx43258Stop/KO mice had gap junction plaques that were larger, but much fewer, and overall gap junction density at the ICD was significantly decreased relative to a

heterozygous Cx43/KO mouse (23). The larger size of individual plaques suggested impaired internalization due to a lack of internalization signals at the C-terminus (4, 24). Therefore, even though there was an exaggerated retention of Cx43 plaque in Cx43258Stop/KO animals, the overall number of plaques was decreased, indicating limited forward trafficking. Combining the findings of the results involving Cx43 with a truncated C-terminus with our direct evidence of the role of internally translated GJA1-20k underlines the role of the C-terminus in promoting forward trafficking to the ICD.

Our study found that the half-lives of WT Cx43 in junctional membrane fraction and non-junctional fraction are 3.43 hours and 2.35 hours, respectively (Figure 6). Both durations are in range of the half-life of Cx43 reported previously (4, 5, 25). However the different half-lives indicate that the cytoplasmic pool of Cx43 is degraded ~50% faster than ICD Cx43. This difference in half-life between the cytoplasmic and the ICD compartments explains the overall reduced Cx43 protein level in the presence of unchanged mRNA (Figures 4 and 5) with GJA1-20k reduction. When forward trafficking is impaired, the Cx43 that does not reach the membrane is more rapidly degraded than Cx43 in the ICDs. Therapeutic interventions that rescue Cx43 forward trafficking will require time for newly synthesized Cx43 to be generated and then trafficked appropriately.

The structural integrity of gap junctions is crucial for the propagation of electrical impulses and synchronized contraction of cardiomyocytes (26, 27). However, *GJA1*$^{M213L/M213L}$ mice were able to live 2-3 weeks despite a significant reduction in the localization of Cx43 at the ICDs of ventricular myocardium (Figures 1E, 3, A and B). In a prior study, mice with cardiac specific

knockout of Cx43 also started to die at 2-3 weeks, and all died within the first two months (28). As with this prior study (28), it is not clear why survival is possible for young mice with reduced Cx43 at their ICD. It is possible that other gap junction proteins might compensate for the lack of Cx43. Mammalian ventricular cardiomyocytes mainly express gap junction proteins Cx43 and Cx45 (29). Although the expression of Cx45 in ventricles is low under normal conditions (29), it will be interesting to examine whether its expression is upregulated in the GJA1-20k knockout mice. Cx45 is a major ventricular connexin during early development and is upregulated in heart failure (30, 31). It is also possible that, under conditions of low cell-cell Cx43 coupling, ephaptic conduction may occur (32). The *GJA1*$^{M213L/M213L}$ mouse may be a novel tool in which to study the potential of ephaptic conduction.

Cx43 has been associated with a host of non-canonical roles, from sperm motility and female reproduction (33, 34), to metabolic function (35), to neurodegenerative diseases (36). There is emerging evidence that GJA1-20k and/or other short Cx43 isoforms (instead of full length Cx43) are involved in these physiological processes and disorders. GJA1-20k has been identified as a stress response protein that targets mitochondria (37) and mediates ischemia-preconditioning (10). There is upregulation of GJA1-20k in rat brain subject to hypoxia (12) and GJA1-20k may be involved in both the myometrium (38) and testicular function (39). Importantly, the results in Figure 7 indicate that the *GJA1*$^{M213L/M213L}$ and *GJA1*$^{M213L/WT}$ mice may represent useful models to further explore the role of GJA1-20k in well recognized but poorly understood non-canonical functions of Cx43.

Our data indicated that the M213L mutation did not significantly change the half-life of the full-length Cx43 protein in either the junctional or non-junctional fraction (Figure 6). It also has been identified that in vitro that the presence of absence of GJA1-20k determines whether Cx43 arrives at cell-cell borders whether WT Cx43 or GJA1-M213L plasmids are used (6). However, it is possible that the M213L mutation affects other biological functions of Cx43, in addition to limiting the translation of GJA1-20k. The GJA1M213L mutant mice, and cells from this mouse, will be a valuable tool to test this possibility.

Taken together, we have developed a *GJA1*$^{M213L/M213L}$ mouse model which effectively removed endogenous GJA1-20k (while preserving full length Cx43) by mutating a single AUG internal ribosomal start site. We have found that the *GJA1*$^{M213L/M213L}$ mice experience severe defects in cardiac electrical coupling, reductions in total Cx43 protein, and sudden death as a result of impaired delivery of full-length Cx43 to the intercalated discs. The significantly shorter life-span of cytosolic Cx43 versus Cx43 at the ICD explains that Cx43 connexons that are not trafficked to the ICD are rapidly degraded and lead to a decrease of overall cellular Cx43 protein.

Emerging data have underscored the stress related upregulation of GJA1-20k and its modulatory effects on ion channel trafficking (6, 7), cytoskeleton organization (7), metabolic regulation (10, 37), and cardioprotection (10). The *GJA1*$^{M213L/M213L}$ mouse model will be useful to explore additional physiological functions of this internally translated protein.

Methods

Generation of the GJA1-M213L knock in founders and genotyping

CRISPR target sequence around the targeted mutation site was selected using the CRISPOR web algorithm (http://crispor.tefor.net) (40). We chose a CRISPR target sequence of ATTCAGAGCGAGAGACACGA followed by a PAM (AGG) of which potential cleavage site is located at 16 bases downstream to the targeted codon (ATG to TTA; M213L). The crRNA (AUUCAGAGCGAGAGACACCAGUUUUAGAGCUAUGCUGUUUUG) and tracrRNA (Cat# U-002000-120) were synthesized by Dharmacon, Inc. (Lafayette, CO). A donor oligo that contains the desired mutation with 60 bases homology arms in both sides that is complementary to the CRISPR target was synthesized by IDT (Coralville, IA). We included a point mutation (TCC to TCG) for disruption of the PAM to avoid reediting after successful induction of homology-directed repair (HDR).

A CRISPR mixture consisted of 25 ng/µl oligo donor, 60 ng/µl crRNA/tracrRNA mix (1:1 molar ratio) and 50 ng/µl eSpCas9 protein (Cat# ESPCAS9PRO-50UG) (Millipore-Sigma, Burlington, MA) was introduced into C57BL/6J (Strain #000664, The Jackson Laboratory, Bar Harbor, ME) fertilized eggs by pronuclear microinjection with a standard method (41). Validation of efficacy of the guide RNA and HDR was performed by PCR genotyping on blastocysts in initial phase and subsequently on tissue samples isolated from transgenic founders and progeny. Briefly, single blastocysts or toe/tail tissue samples were processed and amplified using the KAPA genotyping kit (Cat# KK7352, KAPA Bioscience, Wilmington, MA) with PCR primers (TGGGATTGAAGAACACGGCA and CCACGATAGCTAAGGGCTGG) flanking the targeted mutation site. A 668 bp PCR fragment was isolated from a preparative gel and purified with

QIAquick PCR purification kit (Qiagen, Hilden, Germany) for digestion with NlaIII restriction enzyme. Wild type band segregates into 227 bp and 441 bp fragments because of the native NlaIII site around the targeted site while mutant band remains at 668 bp as this site is destroyed upon successful introduction of desired or undesired mutation(s). Status of introduced mutation(s) was further confirmed by sequencing of the PCR fragments.

We confirmed 9 recombinant mice with heterozygous or mosaic mutations out of 21 mice produced. We established 2 lines (founder lines 37 and 51) after 2 generations of backcrossing with wild type C57BL/6J mice to dilute out possible off-targeting mutations and mosaicism. The 2 lines were used for further expansion of colonies and experiments.

Oligo donor with mutations (underlined):

CCCCACCAGGTGGACTGCTTCCTCTCACGTCCCACGGAGAAAACCATCTTCATCATC

TTCTTACTGGTGGTGTCGTTGGTGTCTCTCGCTCTGAATATCATTGAGCTCTTCTATG

TCTTCTTC

Quantitative RT-PCR

Total RNA was extracted from cardiac ventricular or brain tissues of 2-3 weeks old mice using Trizol per the manufacturer's instruction (Thermo Fisher Scientific, #15596018), followed by an additional purification step with the PureLink RNA mini kit (Thermo Fisher Scientific, #12183018A) and DNase treatment (TURBO™ DNase, Thermo Fisher Scientific, #AM1907). Purified total RNA was reverse transcribed into cDNA with the SuperScript IV VILO master mix (Thermo Fisher Scientific, #11756050). Taqman probes (Thermo Fisher Scientific) to the

mouse *GJA1* (assay ID: Mm00439105-m1), *GAPDH* (assay ID: Mm99999915-g1) genes were used to amplify and detect the corresponding genes. The thermocycling setup is: 2 min at 50ºC; 10 min at 95ºC; 40 cycles of 15 sec at 95ºC and 1 min at 60ºC. Relative expression of the *GJA1* mRNA in mice with different genotypes was normalized to the *GAPDH* mRNA expression level and quantified using the ΔΔCt method.

Immunoprecipitation of Cardiac Cx43 Isoforms

Two to three week old mouse hearts were isolated and perfused with HBSS. Ventricles were homogenized and proteins were extracted in lysis buffer (50 mM Tris pH 8, 5 mM EDTA, 150 mM NaCl, 10 mM KCl, 0.75% Triton X-100, 5 mM NaF, 1 mM $NaVO_3$) supplemented with Halt™ protease and phosphatase inhibitor cocktail (Thermo Fisher Scientific, # 78445) at 4ºC for 2 hours (42). Homogenate was centrifuged at 16,000 x g at 4ºC for 25 min. Lysate supernatant (equivalent to 1.5 mg of protein) was diluted 2-fold with lysis buffer without triton and then pre-cleared with Dynabeads Protein G (Thermo Fisher Scientific, #10004D) at 4ºC for 30 min. Pre-cleared lysate was incubated with 5 ug of mouse anti-Cx43CT1 antibody (Dr. Paul D Lampe, the Fred Hutchinson Cancer Research Center, Seattle, WA) at 4ºC overnight. Samples were subsequently incubated with Dynabeads Protein G at 4ºC for an hour. Immunoprecipitates were washed with buffer (50 mM Tris pH 8, 5 mM EDTA, 150 mM NaCl, 10 mM KCl, 0.25% Triton X-100, 5 mM NaF, 1 mM $NaVO_3$) supplemented with Halt™ protease and phosphatase inhibitor cocktail, then eluted in 2x Sample Buffer. The eluates were subjected to Western blotting.

Western Blotting

Western blotting was performed as described in Basheer et al (7). Protein samples were subjected to SDS-PAGE electrophoresis using NuPAGE Bis-Tris gels (Thermo Fisher Scientific, # NP0335BOX) in MES-SDS running buffer (Thermo Fisher Scientific, # NP0002). NuPAGE Tris-Acetate gels (Thermo Fisher Scientific, # EA0375BOX) and Tris-Aceteate running buffer (Thermo Fisher Scientific, # LA0041) were used for detection of high molecular weight protein such as Nav1.5. The gels were electroblotted onto FluoroTrans polyvinylidene difluoride (PVDF) membranes (Pall Corporation, # BSP0161). For Western blotting with antibodies, membranes were blocked at room temperature with 5% non-fat dry milk (Carnation®) in TNT buffer (50 mM Tris pH 8.0, 150 mM NaCl, 0.1% Tween-20), probed at 4ºC overnight with primary antibodies in blocking buffer, and incubated with fluorophore labeled secondary antibody in blocking buffer at room temperature for an hour. For Western blotting with streptavidin, membranes were blocked at room temperature with 5% BSA (Sigma-Aldrich, #A9647) in TNT buffer, and probed with Alexa-555-Streptavidin (1 to 500 dilution, Thermo Fisher Scientific, #S32355) in blocking buffer at 4ºC overnight.

Western blots were visualized using the ChemiDoc™ MP System and quantified with Image Lab™ software (Bio-Rad) or ImageJ. Primary antibodies used include chicken anti-Cx43 antibody (custom made, detailed below), rabbit anti-Cx43 (1 to 2,000 dilution, Sigma-Aldrich, #C6219), mouse anti-Cx43 antibody (1 to 1,000 dilution, Millipore, #MABT902, clone P2C4), mouse anti-N-cadherin (1 to 1000 dilution, BD biosciences, #610921), rat anti-α-tubulin (1 to 2000 dilution, Abcam, ab6160), rabbit anti-Nav1.5 (1 to 200 dilution, generously provided by Dr. Hugues Abriel at the University of Bern, Bern, Switzerland), and mouse anti-GAPDH (1 to 2000 dilution, Abcam, ab8245).

Generation of Chicken Anti-Cx43 Antibody

A peptide, cdqrpssrassrassrprpddlei, which corresponds to the amino acid sequence 360-382 of the human Cx43 protein and an extra cysteine at the N-terminus, was synthesized (Bio-Synthesis, Texas) and used as the antigen to produce mouse monoclonal antibodies (Epitope Recognition and Immunoreagent Core Facility, University of Alabama at Birmingham). The variable regions of the heavy and light chains of a mouse monoclonal antibody were sequenced and fused with the chicken IgY and chicken lambda-like constant regions, respectively, to generate the chicken anti-Cx43 antibody (Oak Biosciences, Sunnyvale, CA).

ECG Recording and Analysis

Two-three week old mice were anesthetized with isoflurane and positioned in dorsal recumbency position. Electrodes were attached to the left and right forelimbs and left hind limb in a bipolar lead 1 configuration. Electrocardiograms were recorded with the ADInstruments PowerLabs hardware (ADInstruments) for 5 min after 5 min of stabilization of the system. Data were analyzed using the ECG analysis module in LabChart8 software (ADInstruments). The R wave amplitude and QRS duration of each trace were the average values of all the beats in 3-5 minutes of recording. In a case where the software could not detect the correct QRS complexes of a homozygous GJA1-20k knockout mouse, the R wave amplitudes and QRS duration of ≥ 40 beats were manually measured and averaged.

Telemetry Recording and Analysis

Telemetry recording was performed using the DSI MX2 telemetry acquisition system (Data Sciences International) and LabChart8 software (ADInstruments) according to the manufacturer's instruction. Briefly, 6-7 months old adult mice were anesthetized with isoflurane and positioned in dorsal recumbency. A telemetry implant (DSI PhysioTel® ETA-F10 for Mice, Data Sciences International) was surgically placed subcutaneously along the lateral flank, with leads oriented cranially. The ends of the negative and positive leads were tunneled subcutaneously to the right pectoral muscle and left caudal rib region, respectively. Both leads were secured to the abdominal wall with a stay suture. The skin incision was closed with suture. After the mice returned to normal postures and behaviors, their ECG, activities, and temperature were recorded overnight, following their regular light/dark cycles.

Continuous recordings of 3 hours were started between 9 PM and 11 PM in all mice to exclude influences of diurnal rhythms. Data in ASCI format were analyzed with a custom written software using LabView (National Instruments Inc.) and MatLab (The Mathworks, Inc.). Importantly, all ECG complexes were analyzed continuously, first by an automatic algorithm derived from Holter analysis software (Schiller Inc. Baar Switzerland), and subsequently by observing the totality of electrical heart beats on a graphical user interface. Overall, a single data recording of 3 hours included approximately 108'000 electrical hearts beats.

Echocardiography and analysis

Transthoracic echocardiography imaging was performed on anesthetized animals using a VEVO 3100 ultrasound machine with MX5550D transducer (VisualSonics) (10). Left ventricular volume, %EF, and %FS measurements were determined from the B-mode long axis view. LVID,

LVPW, LVAW, heart rate, and left ventricular mass measurements were determined from the M-mode short axis view. E/A and E/e' ratios were measured by Doppler assessment.

Immunostaining, confocal microscopy and quantification of Cx43 at the Intercalated Discs

Cryosections (5 μm) of cardiac ventricular tissues were fixed in pre-chilled acetone for 10 min on ice, blocked and permeabilized at room temperature for an hour in 10% normal goat serum, 2% IgG-free BSA, 0.2% Triton X-100 in 1xPBS. The sections were incubated with primary antibodies in antibody diluent (10% Normal Goat Serum, 0.1% Triton X-100 in 1x PBS) at 4ºC overnight. The sections were then incubated with fluorophore conjugated secondary antibodies (1:500, Thermo Fisher Scientific) and mounted using Fluoromount-G® mounting medium (Southern Biotech, #0100-01). The primary antibodies used were rabbit anti-Cx43 (N-term) (1:100, OriGene, #AP11568PU-N), rabbit anti-Nav1.5 (1:50, kindly gifted from Dr. Hugues Abriel at the University of Bern, Bern, Switzerland) and mouse anti-N-Cadherin (1:100, BD Biosciences, #610921).

The immunostained tissue sections were imaged using a Nikon Eclipse Ti imaging system with a ×60/1.49 Apo objective. Z-stacks (5 μm of total length) of confocal images were obtained.

Quantification of Cx43 or Nav1.5 expression at the intercalated discs (IDs), which were marked by N-Cadherin staining, was performed as previously described (7). Average intensity projection of each stack of confocal images was processed in ImageJ and used to assess protein expression. N-cadherin images were used to generate binary masks of ICDs, which were subsequently

image-multiplied by the corresponding Cx43 image. Cx43 or Nav1.5 fluorescence signal at the ICDs was measured and compared among mice of different genotypes.

Preparation of cardiac ventricular and brain lysates

Mouse cardiac ventricular or brain tissues were homogenized and lysed in RIPA buffer (50 mM Tris, 150 mM NaCl, 1 mM EDTA, 1% TritonX-100, 1% sodium deoxycholate, 1 mM NaF, 0.2 mM Na_3VO_4) supplemented with Halt™ Protease and Phosphatase Inhibitor Cocktail. Samples were incubated at 4ºC for 2 hours, followed by centrifugation at 16,000 x g at 4ºC for 25 min. The lysate supernatant was collected, quantified, and subjected to western blotting.

Triton Solubility Fractionation (in vivo)

Triton fractionation was performed as previously described (18). Briefly, the snap-frozen heart tissues from 2 weeks old mice were homogenized and rotated at 4 °C for 1 hour in 1% Triton X-100 buffer (50 mM Tris pH 7.4, 1% Triton X-100, 2 mM EDTA, 2 mM EGTA, 250 mM NaCl, 1 mM NaF, 0.1 mM Na_3VO_4) with Halt™ protease and phosphatase inhibitor cocktail at a final concentration of 100 mg tissue/ml. The lysates were centrifuged for 20 min. at 10,000 x g in pre-weighed tubes. Supernatant was collected and added to an equal volume of 1% Triton X-100 buffer containing 8 M urea and 2 M thiourea for the soluble fraction. The pellets were weighed and suspended in 1% Triton X-100 buffer containing 4 M urea and 1 M thiourea at a final concentration of 30 mg/ml. NuPAGE sample buffer was added to all fractions followed by sonication. DTT at a final concentration of 100 mM was added and incubate at 37 °C for 20 min. to reduce the samples followed by centrifuge at 10,000 x g for 20 min. The supernatant from soluble or insoluble fraction was subjected to Western blotting described above.

Cloning of Mouse Cx43 Constructs

WT and M213L mutated mouse *GJA1* DNA were amplified from the total cardiac cDNA of a WT and a homozygous GJA1-20k knockout mouse, respectively, using primers that contain sequences resistant to the Cx43 siRNA. The amplicons were cloned into pDONR™221 (Thermo Fisher Scientifics, #12536017) and pcDNA3.2/HA-DEST (9) using Gateway cloning (Thermo Fisher Scientifics) to generate C-terminally HA-tagged constructs.

Primers used in PCR amplification were:

Cx43 Fwd

5'GGGGACAAGTTTGTACAAAAAAGCAGGCTTCGCCGCCACCATGGGTGACTGGAGC GCC 3'

Mouse Cx43 CDS Resist Fwd

5'ATGGGTGACTGGAGCGCCTTGGGGAAGCTGCTGGACAAGGTCCAAGCCTACTCCA CGGCCGGAGGGAAGGTGTGGCTGTCGGTGCTCTTCATTTTCAGAATCCTGCTCCTGG GGACAGCGGTTGAGTCAGCTTGGGGTGACGAACAATCCGCATTCCGCTGTAACACTC AACAACCCG 3'

Mouse Cx43 Rev

5'GGGGACCACTTTGTACAAGAAAGCTGGGTAAATCTCCAGGTCATCAGGCCG 3'

Pulse-Chase Assay with Click-iT Chemistry and Triton Fractionation

HEK293FT cells (Thermo Fisher Scientific) were maintained in Dulbecco's Modified Eagle medium (DMEM) supplemented with 10% FBS, non-essential amino acids, sodium pyruvate (ThermoFisher Scientific) and Mycozap-CL (Lonza, # VZA-2012) unless specified.

Pulse-Chase Assay

Pulse-chase experiment was adapted from the procedure described by James et al (5) with the following modifications. Hek293T cells were reverse transfected with human GJA1 siRNA (ThermoFisher Scientific, Assay ID: HSS178257) (6) at a final concentration of 16 nM using RNAiMax (Thermo Fisher Scientific, # 13778150) and plated in 10 cm dishes. Two days after siRNA transfection siRNA-resistant mouse Cx43 constructs were transfected using FuGENE® HD Transfection Reagent (Promega, # E2312). One day after plasmid transfection, cells were washed and starved for 1 hour in methionine/cysteine-free DMEM (ThermoFisher Scientific, #21013024) supplemented with 10% dialyzed FBS (GE Healthcare, #SH30079.01 or ThermoFisher Scientific, #A3382001). Cells were pulsed for 1 hour with Click-iT L-Azidohomoalanine (ThermoFisher Scientific, #C10102) at a final concentration of 50 μM added in starvation media. Cells were returned to normal growth medium with extra Methionine (1 mM, Sigma-Aldrich, #M5308) and Cysteine (1 mM, Sigma-Aldrich, # C7352). Cells were harvested over a 7.5-hour period at 2.5-hour intervals by centrifuging at 200 x g for 5 min.

Triton Solubility Fractionation (in vitro)

Cell pellet from a 10 cm dish was solubilized in 400 uL of Triton lysis buffer (50 mM Tris, pH7.4, 1% TritonX-100, 2 mM EDTA, 2 mM EGTA, 250 mM NaCl) supplemented with Halt™ protease and phosphatase inhibitor cocktail at 4ºC for an hour. An aliquot of lysate (60 uL) was saved as total protein fraction. The rest of the lysate was centrifuged at 15,000 x g for 30 min. The supernatant and pellet served as the Triton-soluble and -insoluble fractions, respectively.

The total protein fraction was mixed with 4x LDS sample buffer (Thermo Fisher Scientific, # NP0007) with DTT, incubated at 37ºC for 20 min, briefly sonicated, and centrifuged at 10,000 x g for 20 min. The supernatant was subjected to Western blotting.

Immunoprecipitation and Labeling of Pulsed Proteins using Click-iT Chemistry

The Triton-soluble fraction (~340 uL) was sonicated and diluted with 227 uL of Triton lysis buffer without NaCl to reduce salt concentration. The lysate was pre-cleared with Dynabeads Protein G at 4ºC for 30 min and incubated with 3 ug of mouse anti-HA antibody (Abcam, #ab1424, clone 4C12) or 2 ug of rabbit anti-Cx43 antibody (Sigma-Aldrich, #C6219) at 4ºC overnight. Samples were then incubated with Dynabeads Protein G at 4ºC for an hour. Immunoprecipitates were washed 4 x 10 min with wash buffer (50 mM Tris, pH7.4, 1% TritonX-100, 2 mM EDTA, 2 mM EGTA, 150 mM NaCl) supplemented with Halt^{TM} protease and phosphatase inhibitor cocktail. Each immunoprecipitate was washed once and resuspended in 30 uL of 50 mM Tris pH 8. The pulsed proteins in the immunoprecipitate were labeled with Biotin-alkyne using the Click-iT® Biotin Protein Analysis Detection Kit (ThermoFisher Scientific, #C33372) in a final volume of 100 uL according to the manufacturer's recipe at 4ºC for an hour (ThermoFisher Scientific, Click-iT reaction on IP beads-2013JBC). The labeled immunoprecipitate was washed twice in TBS (50 mM Tris-HCl, 150 mM NaCl, pH 7.5). The bound proteins were eluted in 30 µL of 2x LDS buffer with DTT at 37°C for 20 min and subjected to Western blotting. Pulsed and biotin-labeled proteins were detected with Alexa-555-Streptavidin (Thermo Fisher Scientific, #S32355). Total Cx43 in the immunoprecipitates was also probed for with rabbit anti-Cx43 antibody (Sigma-Aldrich, #C6219) or mouse anti-Cx43 antibody (Millipore, #MABT902, clone P2C4).

The Triton-insoluble fraction was re-dissolved in 50 uL of 50 mM Tris-HCl pH7.4, 2% SDS, 1 mM EDTA supplemented with Halt™ protease and phosphatase inhibitor cocktail at 37ºC for 10 min with pipetting. The solubilized fraction was diluted with 7 volume of 150 mM NaCl, 50 mM Tris-HCl pH 7.4, 1mM EDTA, 0.6% NP-40 supplemented with Halt™ protease and phosphatase inhibitor cocktail. The solution was sonicated and centrifuged at 10,000 x g at 4ºC for 20 min. The supernatant was immunoprecipitated and labeled with Click-iT® Biotin-alkyne as described above for the Triton-soluble fraction. The bound proteins were eluted and subjected to Western blotting as described above.

Partition of Newly Synthesized Cx43 in Triton-soluble and -insoluble Fractions

The amount of pulsed Cx43, detected by Streptavidin on a Western blot, at the 0-hr time point was normalized to the amount of total Cx43 in the corresponding immunoprecipitate to account for difference in immunoprecipitation efficiency. The normalized pulsed Cx43 in the Triton-insoluble fraction was divided by that in the Triton-soluble fraction, which served as an indication of the ratio between junctional and non-junctional Cx43. This ratio in cells transfected with the M213L mutated Cx43 is compared to that with the wild type Cx43 to assess the effect of the mutation on delivery of Cx43 to cell-cell junctions.

Quantification of the Time Constant of Full-Length Cx43

The normalized pulsed Cx43, calculated as described above, at different time points during the chase period was divided by that at the 0-hr time point in a specified fraction. Percentages of the remaining normalized pulsed Cx43 were fit with an exponential line in Microsoft Excel. The

time constant (τ) was deduced from the exponential equation, $y = ae^{-t/\tau}$. Half-lives were calculated with the equation, half-life = τ*ln2.

Statistics

All quantitative data were expressed as mean ± SEM. The two tailed Student's t-test, one-way ANOVA with multiple comparisons, two-way ANOVA with multiple comparisons, Kaplan-Meier survival curves and comparisons were performed as appropriate using Prism 6 software (GraphPad). A *P* value less than 0.05 was considered significant.

Study approval

All mice were maintained under sterile barrier conditions. All procedures were reviewed and approved by Cedars-Sinai Medical Center and the University of Utah Institutional Animal Care and Use Committee.

Author contributions

SX, DS, AGK, TTH, and RMS designed research studies. SX, DS, RB, and DMH conducted experiments, acquired data, and analyzed data. SA conducted experiments. YK and MK designed and conducted experiments related to production of knockout mice. PDL provided reagents. AGK analyzed data. SX, DS, and RMS wrote the manuscript. SX, DS, RB, DMH, SA, YK, MK, PDL, AGK, TTH, and RMS reviewed and edited the manuscript. AGK, TTH, and RMS supervised the study.

Acknowledgements

We thank TC Hitzeman for advice on statistical analysis. Dr. Hugues Abriel at the University of Bern generously provided anti-Nav1.5 antibody. This work was supported by NIH/NHLBI grants (AGK-HL136463, TTH-HL133286, RMS-HL138577, RMS-HL152691).

References

1. Basheer W, and Shaw R. The "tail" of Connexin43: An unexpected journey from alternative translation to trafficking. *Biochim Biophys Acta.* 2016;1863(7 Pt B):1848-56.
2. Lo CW. Role of gap junctions in cardiac conduction and development: insights from the connexin knockout mice. *Circ Res.* 2000;87(5):346-8.
3. Saffitz JE. Arrhythmogenic cardiomyopathy and abnormalities of cell-to-cell coupling. *Heart rhythm : the official journal of the Heart Rhythm Society.* 2009;6(8 Suppl):S62-5.
4. Smyth JW, Zhang SS, Sanchez JM, Lamouille S, Vogan JM, Hesketh GG, et al. A 14-3-3 mode-1 binding motif initiates gap junction internalization during acute cardiac ischemia. *Traffic.* 2014;15(6):684-99.
5. James CC, Zeitz MJ, Calhoun PJ, Lamouille S, and Smyth JW. Altered translation initiation of Gja1 limits gap junction formation during epithelial-mesenchymal transition. *Mol Biol Cell.* 2018.
6. Smyth JW, and Shaw RM. Autoregulation of connexin43 gap junction formation by internally translated isoforms. *Cell reports.* 2013;5(3):611-8.
7. Basheer WA, Xiao S, Epifantseva I, Fu Y, Kleber AG, Hong T, et al. GJA1-20k Arranges Actin to Guide Cx43 Delivery to Cardiac Intercalated Discs. *Circ Res.* 2017;121(9):1069-80.
8. Joshi-Mukherjee R, Coombs W, Burrer C, de Mora IA, Delmar M, and Taffet SM. delmar. *Cell communication & adhesion.* 2007;14(2-3):75-84.
9. Smyth JW, Vogan JM, Buch PJ, Zhang SS, Fong TS, Hong TT, et al. Actin cytoskeleton rest stops regulate anterograde traffic of connexin 43 vesicles to the plasma membrane. *Circ Res.* 2012;110(7):978-89.
10. Basheer WA, Fu Y, Shimura D, Xiao S, Agvanian S, Hernandez DM, et al. Stress response protein GJA1-20k promotes mitochondrial biogenesis, metabolic quiescence, and cardioprotection against ischemia/reperfusion injury. *JCI Insight.* 2018;3(20).
11. Salat-Canela C, Sese M, Peula C, Ramon y Cajal S, and Aasen T. Internal translation of the connexin 43 transcript. *Cell communication and signaling : CCS.* 2014;12:31.
12. Ul-Hussain M, Olk S, Schoenebeck B, Wasielewski B, Meier C, Prochnow N, et al. Internal Ribosomal Entry Site (IRES) Activity Generates Endogenous Carboxyl-terminal Domains of Cx43 and Is Responsive to Hypoxic Conditions. *The Journal of biological chemistry.* 2014;289(30):20979-90.
13. Reaume AG, de Sousa PA, Kulkarni S, Langille BL, Zhu D, Davies TC, et al. Cardiac malformation in neonatal mice lacking connexin43. *Science.* 1995;267(5205):1831-4.
14. Bacharova L, Mateasik A, Krause R, Prinzen FW, Auricchio A, and Potse M. The effect of reduced intercellular coupling on electrocardiographic signs of left ventricular hypertrophy. *J Electrocardiol.* 2011;44(5):571-6.
15. Danik SB, Liu F, Zhang J, Suk HJ, Morley GE, Fishman GI, et al. Modulation of cardiac gap junction expression and arrhythmic susceptibility. *Circ Res.* 2004;95(10):1035-41.
16. Morley GE, Danik SB, Bernstein S, Sun Y, Rosner G, Gutstein DE, et al. Reduced intercellular coupling leads to paradoxical propagation across the Purkinje-ventricular junction and aberrant myocardial activation. *Proc Natl Acad Sci U S A.* 2005;102(11):4126-9.

17. Bacharova L, Plandorova J, Klimas J, Krenek P, and Kyselovic J. Discrepancy between increased left ventricular mass and "normal" QRS voltage is associated with decreased connexin 43 expression in early stage of left ventricular hypertrophy in spontaneously hypertensive rats. *J Electrocardiol.* 2008;41(6):730-4.
18. Smyth JW, Hong TT, Gao D, Vogan JM, Jensen BC, Fong TS, et al. Limited forward trafficking of connexin 43 reduces cell-cell coupling in stressed human and mouse myocardium. *The Journal of clinical investigation.* 2010;120(1):266-79.
19. Asimaki A, Tandri H, Huang H, Halushka MK, Gautam S, Basso C, et al. A new diagnostic test for arrhythmogenic right ventricular cardiomyopathy. *The New England journal of medicine.* 2009;360(11):1075-84.
20. Shaw RM, Fay AJ, Puthenveedu MA, von Zastrow M, Jan YN, and Jan LY. Microtubule plus-end-tracking proteins target gap junctions directly from the cell interior to adherens junctions. *Cell.* 2007;128(3):547-60.
21. Shaw RM, and Rudy Y. Ionic mechanisms of propagation in cardiac tissue. Roles of the sodium and L-type calcium currents during reduced excitability and decreased gap junction coupling. *Circ Res.* 1997;81(5):727-41.
22. Maass K, Ghanem A, Kim JS, Saathoff M, Urschel S, Kirfel G, et al. Defective epidermal barrier in neonatal mice lacking the C-terminal region of connexin43. *Mol Biol Cell.* 2004;15(10):4597-608.
23. Maass K, Shibayama J, Chase SE, Willecke K, and Delmar M. C-terminal truncation of connexin43 changes number, size, and localization of cardiac gap junction plaques. *Circ Res.* 2007;101(12):1283-91.
24. Remo BF, Qu J, Volpicelli FM, Giovannone S, Shin D, Lader J, et al. Phosphatase-resistant gap junctions inhibit pathological remodeling and prevent arrhythmias. *Circ Res.* 2011;108(12):1459-66.
25. Beardslee MA, Laing JG, Beyer EC, and Saffitz JE. Rapid turnover of connexin43 in the adult rat heart. *Circ Res.* 1998;83(6):629-35.
26. Delorme B, Dahl E, Jarry-Guichard T, Briand JP, Willecke K, Gros D, et al. Expression pattern of connexin gene products at the early developmental stages of the mouse cardiovascular system. *Circ Res.* 1997;81(3):423-37.
27. Kasi VS, Xiao HD, Shang LL, Iravanian S, Langberg J, Witham EA, et al. Cardiac-restricted angiotensin-converting enzyme overexpression causes conduction defects and connexin dysregulation. *Am J Physiol Heart Circ Physiol.* 2007;293(1):H182-92.
28. Gutstein DE, Morley GE, Tamaddon H, Vaidya D, Schneider MD, Chen J, et al. Conduction slowing and sudden arrhythmic death in mice with cardiac-restricted inactivation of connexin43. *Circ Res.* 2001;88(3):333-9.
29. van Veen TAB, van Rijen HVM, and Opthof T. Cardiac gap junction channels: modulation of expression and channel properties. *Cardiovascular Research.* 2001;51(2):217–29.
30. Vaidya D, Tamaddon HS, Lo CW, Taffet SM, Delmar M, Morley GE, et al. Null mutation of connexin43 causes slow propagation of ventricular activation in the late stages of mouse embryonic development. *Circ Res.* 2001;88(11):1196-202.
31. Yamada KA, Rogers JG, Sundset R, Steinberg TH, and Saffitz JE. Up-regulation of connexin45 in heart failure. *J Cardiovasc Electrophysiol.* 2003;14(11):1205-12.

32. Veeraraghavan R, Gourdie RG, and Poelzing S. Mechanisms of cardiac conduction: a history of revisions. *Am J Physiol Heart Circ Physiol.* 2014;306(5):H619-27.
33. Kidder GM, and Cyr DG. Roles of connexins in testis development and spermatogenesis. *Semin Cell Dev Biol.* 2016;50:22-30.
34. Winterhager E, and Kidder GM. Gap junction connexins in female reproductive organs: implications for women's reproductive health. *Hum Reprod Update.* 2015;21(3):340-52.
35. Rodriguez-Sinovas A, Ruiz-Meana M, Denuc A, and Garcia-Dorado D. Mitochondrial Cx43, an important component of cardiac preconditioning. *Biochim Biophys Acta Biomembr.* 2018;1860(1):174-81.
36. Freitas-Andrade M, and Naus CC. Astrocytes in neuroprotection and neurodegeneration: The role of connexin43 and pannexin1. *Neuroscience.* 2016;323:207-21.
37. Fu Y, Zhang SS, Xiao S, Basheer WA, Baum R, Epifantseva I, et al. Cx43 Isoform GJA1-20k Promotes Microtubule Dependent Mitochondrial Transport. *Front Physiol.* 2017;8:905.
38. Nadeem L, Shynlova O, Mesiano S, and Lye S. Progesterone Via its Type-A Receptor Promotes Myometrial Gap Junction Coupling. *Sci Rep.* 2017;7(1):13357.
39. Kubincova P, Sychrova E, Raska J, Basu A, Yawer A, Dydowiczova A, et al. Polycyclic Aromatic Hydrocarbons and Endocrine Disruption: Role of Testicular Gap Junctional Intercellular Communication and Connexins. *Toxicol Sci.* 2019;169(1):70-83.
40. Haeussler M, Schonig K, Eckert H, Eschstruth A, Mianne J, Renaud JB, et al. Evaluation of off-target and on-target scoring algorithms and integration into the guide RNA selection tool CRISPOR. *Genome Biol.* 2016;17(1):148.
41. Behringer R, Gertsenstein M, Nagy KV, and Nagy A. *Manipulating the mouse embryo : a laboratory manual.* Cold Spring Harbor, New York: Cold Spring Harbor Laboratory Press; 2014.
42. Fu Y, Shaw SA, Naami R, Vuong CL, Basheer WA, Guo X, et al. Isoproterenol Promotes Rapid Ryanodine Receptor Movement to Bridging Integrator 1 (BIN1)-Organized Dyads. *Circulation.* 2016;133(4):388-97.

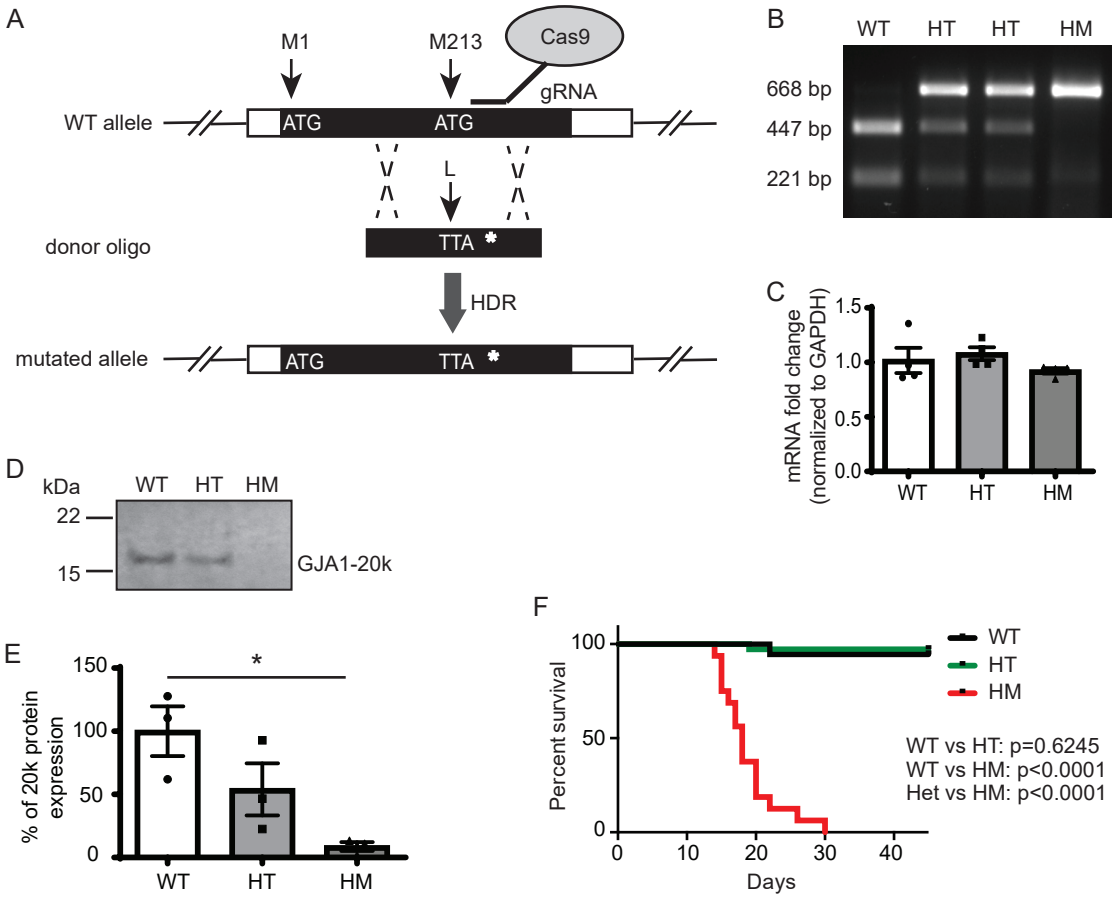

Figure 1. Generation of the M213L mouse model and survival of the mutant mice.

(**A**) schematic diagram showing the site-directed mutation of ATG, encoding M213, to TTA, encoding an L, at the *GJA1* genomic locus using CRISPR technology. HDR: homology directed repair. (**B**) Representative genotyping results confirm presence of the M213L mutation in 0, 1, and both copies of the *GJA1* gene in WT mice, heterozygous (HT), and homozygous (HM) for M213L, respectively. (**C**) Quantification of the *GJA1* mRNA expression in the hearts of WT, HT, HM mice. One-way ANOVA, with n = 4 in each group. Data represents mean ± SEM. (**D**) Representative western blot showing the expression of GJA1-20k protein in cardiac ventricles of WT, HT, and HM mice (2-3 weeks old) after immunoprecipitation. n = 3 experiments. (**E**) Quantification of GJA1-20k protein expression in cardiac ventricles of 2-3 weeks old mice among genotypes. Kruskal-Wallis test, followed by Dunn's multiple comparisons, with n = 3 in each group. Data represents mean ± SEM. (**F**) Kaplan-Meier survival curve of the WT (n = 18, black), HT (n = 36, green), and HM (n = 16, red) mice. Survival curves were compared using Log-rank (Mantel-Cox) test.

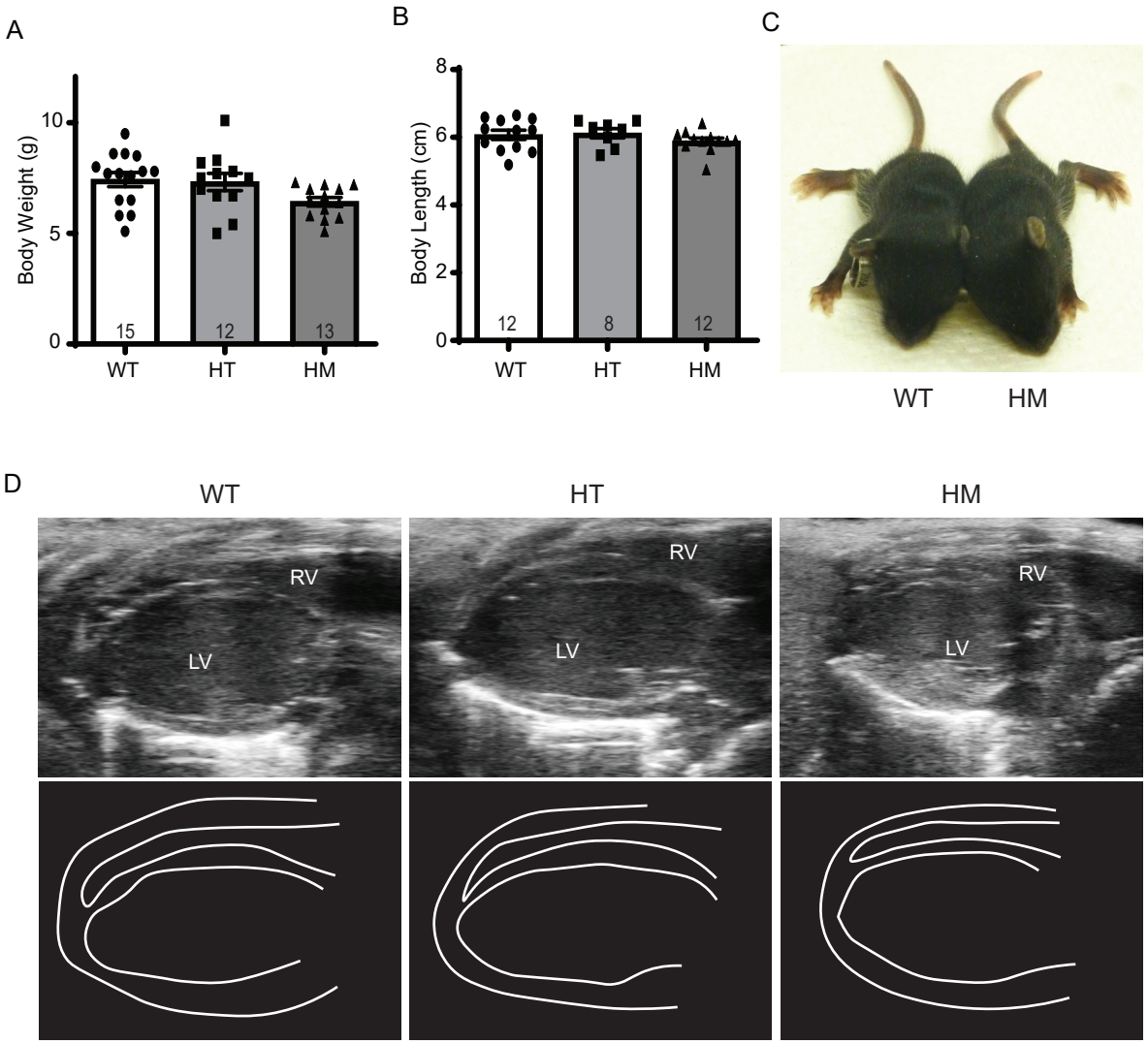

Figure 2. Morphology of the hearts and gross physical parameters of young (2-3 weeks old) M213L mice.

(**A** and **B**) Quantification of body weight (**A**) and body length (**B**) of WT, HT, and HM mice. (**C**) A representative image of a WT and HM mice. (**D**) Representative long axis echocardiograph images of young WT, heterozygous (HT), and homozygous (HM) mice. The lower panels indicate the trace images of heart wall. LV, left ventricle; RV, right ventricle. One-way ANOVA test. The number of mice (n) in each group is indicated within bars or Table 1. Data represents mean ± SEM.

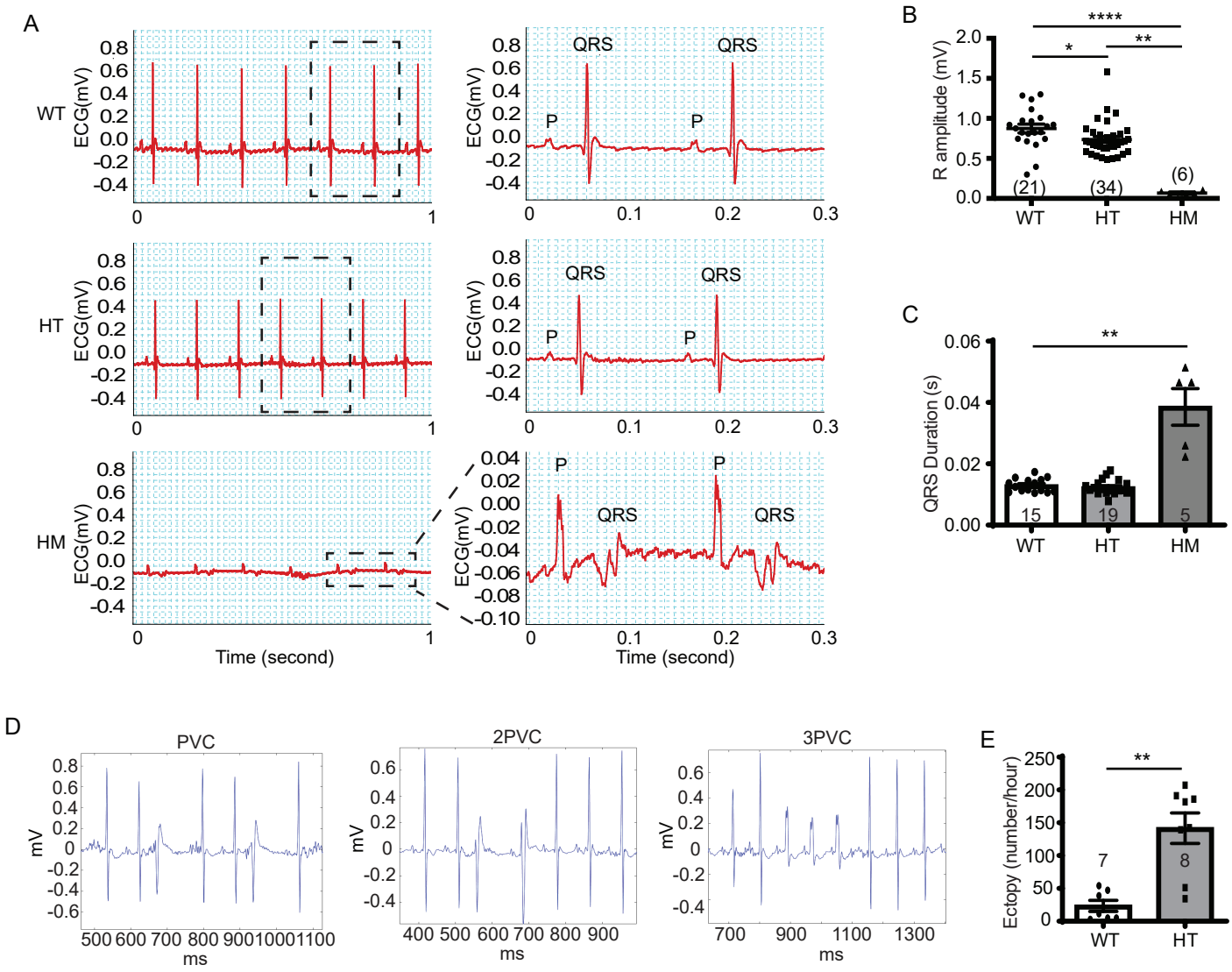

Figure 3. Electrocardiograms (ECG) of young (14-22 days) and adult (6-7 months) M213L mice. (**A**) Representative ECG traces of anesthetized young WT, heterozygous (HT), and homozygous (HM) mice. Quantification of the amplitude of R waves (**B**) and QRS duration (**C**) in young WT, HT, and HM mice. Kruskal-Wallis test, followed by Dunn's multiple comparisons. (**D**) Examples of 1, 2, and 3 consecutive premature ventricular contractions (PVC) occurred in adult HT mice during the dark cycle recorded by telemetry. (**E**) Quantification of the number of PVC incidents in adult WT and HT mice. Mann-Whitney test with two-tailed P value. (**C-E**) Data represents mean ± SEM. * $p \leq 0.05$, ** $p \leq 0.01$, **** $p \leq 0.0001$. The number of mice (n) in each group is indicated in parentheses or within bars.

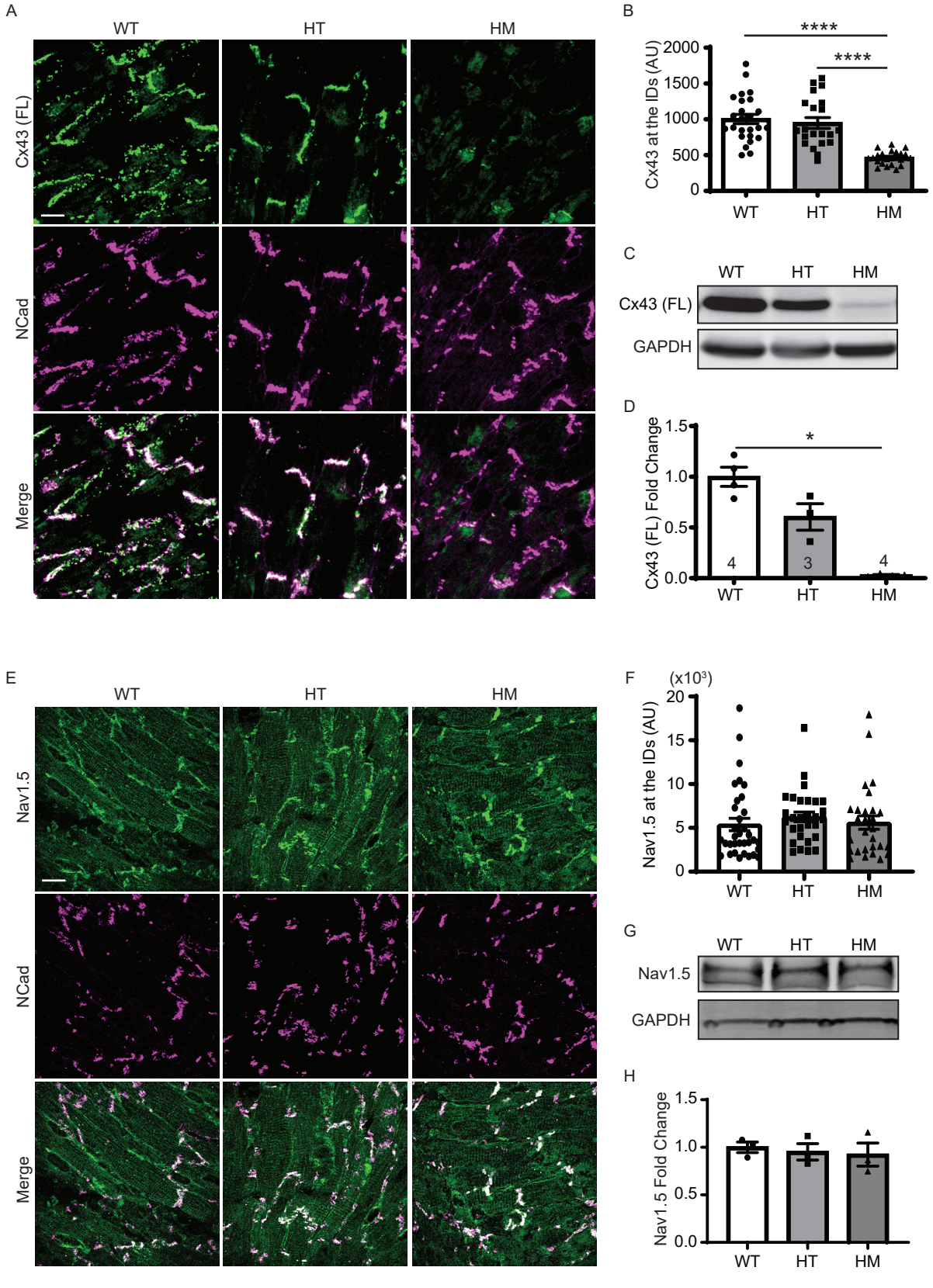
A
WT
HT
HM
Cx43 (FL)
NCad
Merge
B
Cx43 at the IDs (AU)
2000
1500
1000
500
0
****
****
WT
HT
HM
C
WT
HT
HM
Cx43 (FL)
GAPDH
D
Cx43 (FL) Fold Change
1.5
1.0
0.5
0.0
*
4
3
4
WT
HT
HM
E
WT
HT
HM
Nav1.5
NCad
Merge
F
(x10³)
Nav1.5 at the IDs (AU)
20
15
10
5
0
WT
HT
HM
G
WT
HT
HM
Nav1.5
GAPDH
H
Nav1.5 Fold Change
1.5
1.0
0.5
0.0
WT
HT
HM

Figure 4. Localization and expression of full-length Cx43 and Nav1.5 in cardiac ventricles of young (2-3 weeks old) M213L mice.

(**A** and **E**) Representative average projected immunofluorescence images of N-cadherin (NCad), full-length (FL) Cx43 (**A**), and Nav1.5 (**E**), in cryosections of cardiac ventricles. Cx43 and Nav1.5 are shown in green, and NCad is shown in magenta. Co-localization is shown as white in the merged images. Scale bar = 15 μm. (**B** and **F**) Quantification of the immunofluorescence signal of Cx43 (FL) (**B**) and Nav1.5 (**F**) at the intercalated discs that are identified with NCad. **** $p \leq 0.0001$, Kruskal-Wallis test, followed by Dunn's multiple comparisons, n = 25, 21, and 22 images (**B**) and n = 34, 29, and 28 images (**F**) of WT, heterozygous (HT), and homozygous (HM) mice, respectively, with 6 mice in each group. Data represents mean ± SEM. (**C** and **G**) Representative Western blots showing the expression of Cx43 (FL) (**C**) and Nav1.5 (**G**) protein in the cardiac ventricles of WT, HT, and HM mice. n = 3 experiments. (**D** and **H**) Quantification of Cx43(FL) (**D**) and Nav1.5 (**H**) protein expression. The values were normalized to GAPDH expression. All graph data represents mean ± SEM. * $p \leq 0.05$, Kruskal-Wallis test, followed by Dunn's multiple comparisons, n = 3 mice in each group.

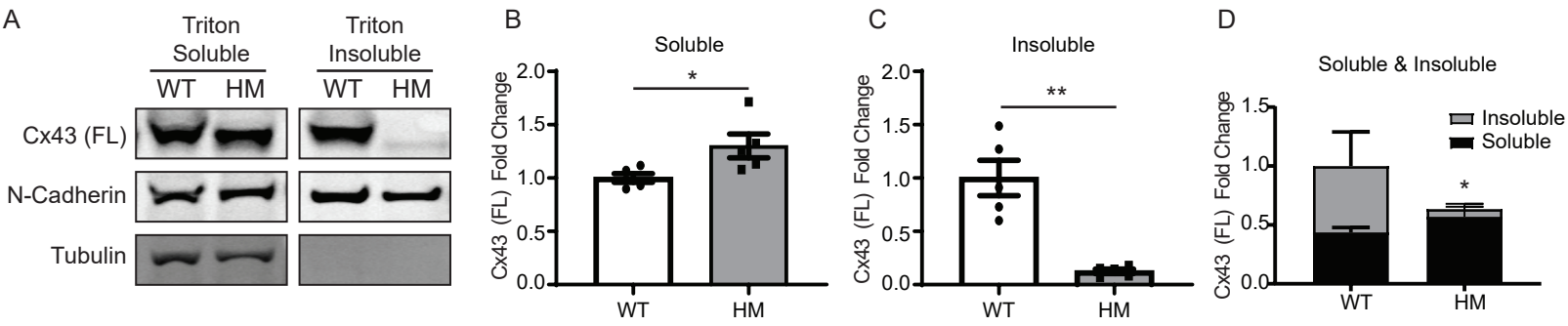

Figure 5. Cx43 expression in triton soluble (cytoplasmic) and insoluble (junctional membrane) fractions in young (2-3 weeks old) mouse hearts.

(**A**) Representative Western blots showing the expression of Cx43 (FL), N-cadherin, and Tubulin. (**B** and **C**) The quantification of graphs of Cx43 (FL) expression in soluble (**B**) and insoluble (**C**) fractions from WT and homozygous (HM) mouse hearts. The insoluble fraction of Cx43 (FL) was drastically decreased in HM. (**D**) The fold change of Cx43 (FL) in total (both soluble and insoluble). All graph data represents mean ± SEM. * $p \leq 0.05$, ** $p \leq 0.01$ Mann-Whitney test with two-tailed *P* value. n = 5 mice in each group.

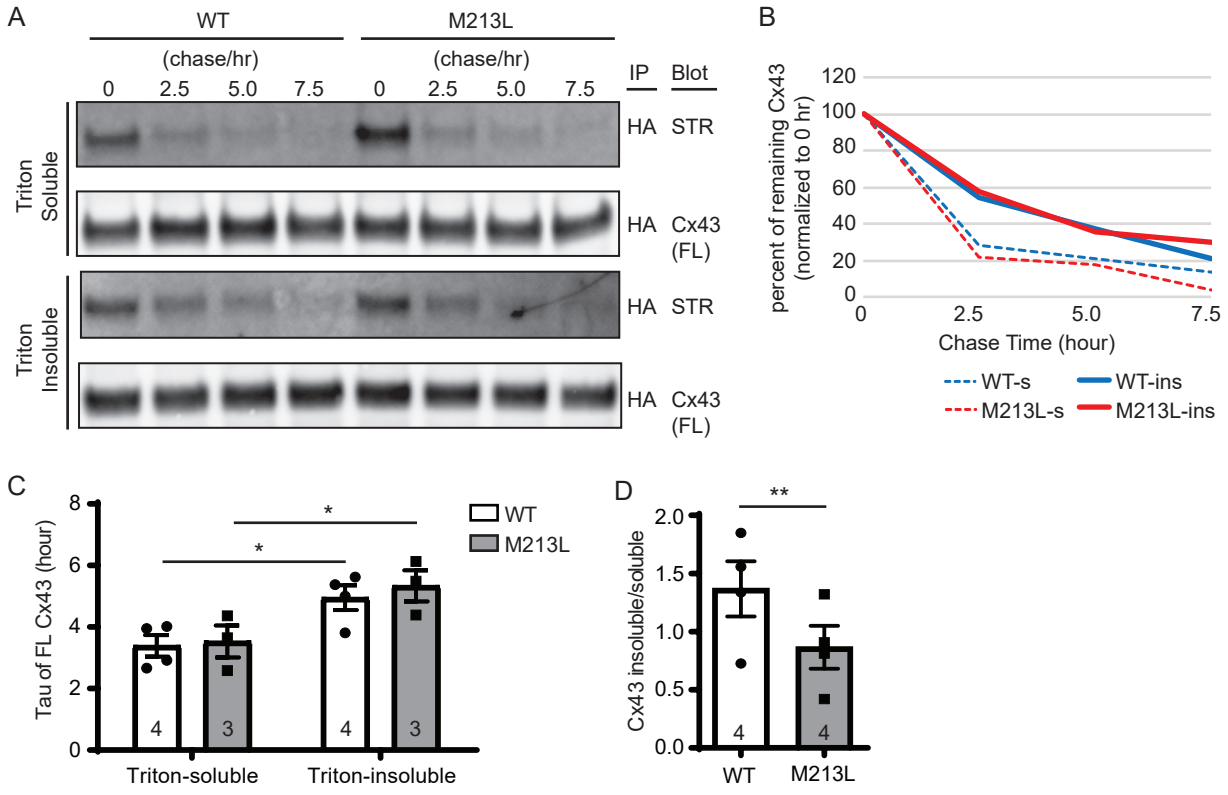

Figure 6. Stabilities of exogenous WT and M213L Cx43 protein in HEK cells.

(**A**) Representative western blots of the immunoprecipitated (IP), pulsed (blotted with Streptavidin (STR)) and total (blotted with Cx43 antibody) exogenously expressed full-length Cx43 (FL) in Triton-soluble and -insoluble fractions at various time points during the chase period. n = 4 and 3 independent experiments for the WT and M213L mutated protein, respectively. (**B**) Plots of the decay of full-length Cx43 proteins shown in (**A**). (**C**) Quantification of Tau, time constant of full-length Cx43, of WT and M213L mutated protein in triton-soluble and -insoluble fractions. * $p \leq 0.05$, two-way ANOVA, followed by Fisher's LSD multiple comparisons. n = 4 and 3 independent experiments for the WT and M213L mutated protein, respectively. (**D**) Quantification of the ratio of pulsed full-length Cx43 in Triton-insoluble over Triton-soluble fraction at the start of the chase period (0 hr time point). ** $p \leq 0.01$, paired t-test with two-tailed *P* value. n = 4 independent experiments. (**C-D**) Data represents mean ± SEM.

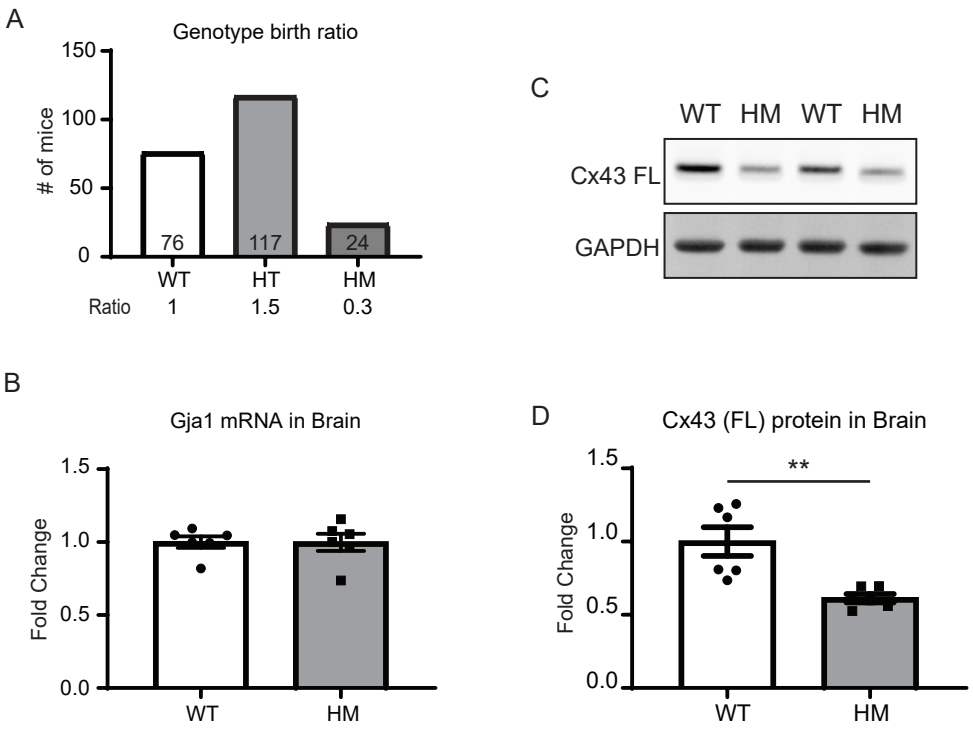

Figure 7. The effects of M213L mutation on birth ratio and brain Cx43 expression.

(**A**) Quantification of the number of WT, heterozygous (HT), and homozygous (HM) mice born within 6 months. The ratio is significantly different from that of the Mendelian inheritance. $p \leq 0.0001$ in a Chi-square test. The number of mice (n) of each genotype is indicated within bars. (**B** and **D**) The expression levels of the *GJA1* mRNA (**B**) and Cx43 protein (**D**) in the brain from WT and HM mice. The data were normalized by GAPDH expression. (**C**) Representative Western blots showing Cx43 (FL) and GAPDH expression in the brain. All graph data represents mean ± SEM. ** $p \leq 0.01$ Mann-Whitney test with two-tailed *P* value. n = 6 mice in each group.